Applied Nanoscience (2020) 10:4013–4027
https://doi.org/10.1007/s13204-020-01510-y

ORIGINAL ARTICLE

Fabrication and optimization of pH-sensitive mannose-anchored nano-vehicle as a promising approach for macrophage uptake

Mahwash Mukhtar[1,2] · Mahira Zesshan[1] · Salman Khan[1] · Gul Shahnaz[1] · Saeed Ahmad Khan[3] · Hafiz Shoaib Sarwar[1,4] · Riffat Asim Pasha[5] · Hussain Ali[1]

Received: 24 April 2020 / Accepted: 8 July 2020 / Published online: 17 July 2020

Abstract

Mannose receptors (MR) are highly over-expressed on macrophages in the inflammatory bowel disease (IBD) and can be targeted by developing mannose-anchored nano-carrier system. In this study, mannosylated chitosan (MC) polymer was synthesized because of its high affinity for mannose receptors. Afterward, MC nanoparticles (NPs) were fabricated encapsulating dexamethasone to target macrophages for attenuation of inflammation at initial stages. Further, NPs were coated with a pH-sensitive polymer to control the premature drug release in the stomach. NPs were optimized using a surface response quadratic model to study the impact of various process parameters. Optimized NPs were then characterized for size, morphology, zeta potential, surface chemistry, biocompatibility, and uptake by macrophages. The average particle size was found to be 380 ± 19.8 nm with an encapsulation efficiency of $78.1 \pm 1.17\%$. pH-dependent drug release profile was obtained with an average release of $73.9 \pm 5.24\%$ over 72 h in simulated intestinal fluid (pH 7.4). Moreover, the NPs uptake by the macrophages supported the viability of macrophages with the NPs and did not show any adverse effects. Moreover, this study was supported by the uptake of NPs inside macrophages. Altogether, the data supported that MC NPs could serve as a potential anti-inflammatory therapeutic approach to target macrophages in IBD.

Keywords Factorial design · Kinetics · Nanotechnology · Mannosylated chitosan · Polymer synthesis · Surface chemistry

Abbreviations

CD	Crohn's disease
DEXA	Dexamethasone
DSC	Differential scanning calorimetry
EE	Encapsulation efficiency
ES100	Poly (methacrylic acid-co-methyl methacrylate) 1:2, Eudragit® S100
FBS	Fetal bovine serum
FTIR	Fourier transform infrared spectroscopy
GIT	Gastrointestinal tract
IBD	Inflammatory bowel disease
IRFs	Interferons
MC	Mannosylated chitosan
MR	Mannose receptor
NF-κB	Nuclear factor-kappa activated B cells
NPs	Nanoparticles
PAF	Platelet activating factor
PAMPs	Pathogen-associated molecular patterns
PDI	Polydispersity index
PRRs	Pattern recognition receptors
Rh-B	Rhomadine B
SEM	Scanning electron microscope
SGF	Simulated gastric fluid
SIF	Simulated intestinal fluid
TC	Thiolated chitosan
TGA	Thioglycolic acid

Electronic supplementary material The online version of this article (https://doi.org/10.1007/s13204-020-01510-y) contains supplementary material, which is available to authorized users.

✉ Hussain Ali
h.ali@qau.edu.pk

[1] Department of Pharmacy, Faculty of Biological Sciences, Quaid-i-Azam University, Islamabad 45320, Pakistan

[2] Faculty of Pharmacy, Institute of Pharmaceutical Technology and Regulatory Affairs, University of Szeged, Eötvös utca 6, Szeged 6720, Hungary

[3] Department of Pharmacy, Kohat University of Science and Technology, Kohat 26000, Pakistan

[4] Riphah Institute of Pharmaceutical Sciences, Riphah International University, Lahore Campus, Lahore, Pakistan

[5] Department of Mechanical Engineering, University of Engineering and Technology Taxila, Rawalpindi, Pakistan

UC Ulcerative colitis
XPS X-ray photon spectroscopy

Introduction

Inflammatory bowel disease (IBD) is a chronic relapsing disorder of gastrointestinal tract (GIT), with two major types; ulcerative colitis (UC) and Crohn's disease (CD). These two types somehow share a genetically similar background but vary in affecting the depth of the intestinal layer and mode of progression (Sartor 2006). UC usually affects tissues of the colon and rectum and exhibits a continuous pattern. On the contrary, the CD can be present anywhere in gastrointestinal tract GIT) but most commonly exists in ileum and colon (Beaugerie et al. 2018).

Moreover, IBD is either the autoimmune response against microbiota or mucosal antigens or it might be due to the immune system's defensive mechanism to protect the body from invading pathogens. If the process of acute inflammation is prolonged, it may lead to chronic disorders. Among inflammatory scavengers, macrophage plays a vital role in IBD. During the initial phase of inflammation, macrophages derived from circulating monocytes accumulate in the colon tissue. These macrophages can identify pathogen-associated molecular patterns (PAMPs) on the antigens through their pattern recognition receptors (PRRs). After binding of PAMPs to PRRs, a cascade of pro-inflammatory cytokines and chemokines bursts, along with an increased infiltration of nuclear factor kappa-activated B cells (NF-κB) and interferons (IRFs) in inflamed tissues of the colon (Akira et al. 2006). One of the PRRs is mannose receptor (MR), which is highly sensitive to repeating mannose residues and has been investigated as a novel target for the drug delivery strategies in inflammation. MR scrutinizes the mannose rich, cysteine-rich NH_2 compounds, sulfated moieties (glycoproteins), and hydroxyl groups of hexose sugars (Mukhtar et al. 2020).

Conferring to the treatment of IBD, corticosteroids are the firstline therapy; however, severe side effects limited their use. Among corticosteroids, 9-fluoro glucocorticoid, i.e., dexamethasone, (DEXA) is the most potent drug of choice which exhibits its anti-inflammatory role through inhibitory protein, phospholipase A2. DEXA suppresses inflammation by reducing capillary permeability and pro-inflammatory mediators like platelet-activating factor (PAF), prostaglandins, eicosanoids, and thromboxane. DEXA can up-regulate the MR expression on the surface of macrophage (Chakraborty et al. 2001) and has been explored in the past for treating the inflammatory disorder. However, a high dose of DEXA may cause abdominal distention and intestinal perforations, it is, therefore, necessary to optimize its dose for IBD treatment, mucosal tissue remodeling and healing (Tams Todd 2003). Mostly, orally administered IBD therapeutic regimen encounters adverse effects and therapeutic failures due to drug leakage in upper parts of GIT, increased clearance rate from the bowel, dose-dependent toxicity, pre-systemic absorption, and inability to deliver the drug at targeted tissues of the colon. The resultant outcome is inability to achieve the state of remission and maintenance of remission. To overcome this problem, an effective oral drug delivery system should be designed which avoids off-site targeting and concentrate the drug in the colon. One of the solutions is to utilize a pH-dependent and targeted drug delivery system to protect the drug from the harsh environment of GIT and adhere to the intestinal mucosa for prolonged drug release (Zeeshan et al. 2019a).

Since, nanotechnology provides better therapeutics for IBD by delivering the nano-scale particles to an inflamed area of colon with enhanced site retention, reduced tissue toxicity, and lower systemic side effects (Giron et al. 2019). Nanoparticles with decreased nano-size range and cationic surface charge have more affinity for the inflamed mucosal surface (Vafaei et al. 2016). Since macrophage function is associated with inflammation, developing a system capable of targeting macrophages and modulating their role may be a promising treatment approach. Recently, muco adhesive mannose-anchored polymeric NPs have been delivered to the macrophages under inflamed conditions (Hatami et al. 2019). Previously, mannosylated chitosan (MC) NPs have been explored for systemic delivery based on the concept of immunization.

The present study aimed to design NPs using MC, derived from chitosan (a biocompatible and non-toxic linear polysaccharide, comprising of repeating units of D-glucosamine and *N*-acetyl-D-glucosamine). MC is a cationic polysaccharide with a high affinity for MR on macrophage and negatively charged mucin of epithelium of GIT; therefore, this strategy is assumed to be effective in IBD. Furthermore, MC NPs were coated with anionic pH-sensitive polymer, to deliver the drug specifically to colon and to inhibit drug release in the stomach (Ali et al. 2014).

Materials and method

Materials

Dexamethasone (MW = 392.46 g/mol), sodium tri-polyphosphate (TPP), low molecular weight chitosan (MW = 10 kD, degree of deacetylation = 75–85%), cysteine and thioglycolic acid (TGA) were purchased from Sigma Aldrich (Sigma Aldrich, St. Louis, MO). Poly(methacrylic acid-co-methyl methacrylate) 1:2, Eudragit® S100(ES100) was provided by Evonik® industries (Darmstadt, Germany), acetone (AnalaR Chemicals Ltd, England), hydroxylamine chloride and Tween-80 (Merck, Germany), ethanol (BDH laboratory

supplies, England) and D-Mannose (Avonchemlimited, UK), 3-(4,5-dimethylthaizol-2-yl)-2,5-diphenyltetrazolium bromide (MTT) from Amresco.

Synthetic procedure for polymer and nanoparticles preparation

Synthesis of thiolated chitosan (TC) polymer

1% chitosan (CS) solution was prepared in 0.5% acetic acid solution. Then 6.89 ml of TGA (giving approximately conc. of 500 mg of TGA) was added slowly to the prepared polymeric solution, followed by the addition of 50 mM EDAC (1-ethyl-3-3(3-dimethylaminopropyl) carbodiimide hydrochloride)). Meanwhile, the mixture was kept on stirring. 50 mM hydroxylamine chloride solution was added with continuous shaking to prevent oxidation. The pH of the mixture was maintained to 5.8, which was later incubated at room temperature for approximately 4 h. Afterward, the mixture was dialyzed in dialysis membrane (molecular weight cutoff 12–14 kDa) at 10 °C in dark, by changing media after every 6 h to remove any unbound content from TGA. Dialysis medium was changed intermittently in the following manner, (5L of 5 mM HCl solution, 5L of 5 mM HCL for another 6 h, 5L of 5 mM HCl with 1% NaCl (according to the volume of polymer solution in 1:1 ratio), repetition of the same medium for another 6 h, 1 mM HCl and finally with 1 mM HCl for 6 h at pH 4). The final mixture was removed from dialysis bags and frozen at − 80 °C and lyophilized. After lyophilization, a white amorphous mass was obtained which was then stored at 4 °C for further use.

Synthesis of mannosylated chitosan (MC) polymer

Mannosylated chitosan was then synthesized by immobilization of mannose groups on thiolated chitosan (Afzal et al. 2019). 2% TC solution was prepared in 0.5% glacial acetic acid. To aid the process of reductive amination, 0.12 M cyanoborohydride was added followed by the addition of 0.33 M D-mannose with continuous stirring. The viscous polymeric solution was formed which was then washed with 150 ml methanol four times and 150 ml diethyl ether once using a dialysis membrane (molecular weight cutoff 12–14 kDa). Pinkish polymeric mass was obtained, which was lyophilized and stored in light-resistant and moisture-resistant environment.

Thiol groups determination in chitosan-TGA conjugate

The number of thiol groups' immobilization to chitosan structure determines the degree of conjugation. Conjugation of thiol groups to TC and MC was determined using Ellman's reagent (Afzal et al. 2019). Approximately 0.5 mg of TC and MC were hydrated in deionized water separately. 500 µl of phosphate buffer (pH 8) and 500 µl of Ellman's reagent were added in both suspensions, which were then incubated at room temperature for 3 h. Mixtures were then centrifuged at 24,000 rpm for 5 min to obtain supernatant. Absorbance was then estimated at 430 nm wavelength (using microfiltration plate reader, Perkin Elmer), measured against TGA standard, to calculate the number of thiol groups immobilized on polymer.

Determination of disulfide bonds

Disulfide bond determination was performed to quantify the number of free thiol groups on TC and MC (Bernkop-Schnürch et al. 1999). 0.5 mg of conjugated polymers were dissolved in distilled water. 650 µl of phosphate buffer (pH 6.8) and 1 ml of sodium borohydride solution were added into the polymer solutions and incubated at room temperature for 1 h. 5 M HCl (200 µl) was then mixed in the incubated suspensions to degrade the remaining amount of sodium borohydride. Ellman's reagent (0.4%w/v) was added to determine the remaining free thiol groups. The absorbance of samples was measured at 450 nm wavelength using a microtitration plate reader.

Disulfide content was determined by subtracting the no. of unattached thiol groups from total no. of conjugated thiol groups.

Determination of mannose groups

The number of mannose groups immobilized on MC was quantified by the method reported (Dehshahri et al. 2012). In brief, 4 mg of the polymer was dissolved in 2 ml of distilled water. 20 µl of this polymeric solution was placed in 96 well plate and 20 µl of resorcinol, 100 µl of sulfuric acid and 50 µl of pristane (2,6,10,14-tetramethyl-pentadecane) was added to well plates. Well plates were kept on vortex for constant shaking, and then the plates were transferred to the oven (90 °C) for 30 min in the darkroom. Optical density at 450 nm wavelength was determined using a microtitration plate reader. Mannose concentration was determined in this way. A schematic synthesis of polymer is shown in Fig. 1.

Preparation of uncoated dexamethasone-loaded mannosylated chitosan (MC/DEXA) nanoparticles

Nanoparticles were synthesized through the ionic gelation method using cross-linker TPP. Polymer solution was prepared by dissolving 1% (w/v) of MC in 0.05 M glacial acetic acid (GAA). 1 ml of TPP (0.1% w/v) was then added dropwise in a 5 ml polymer solution until a bluish haze appeared. 0.5% (w/v) poloxamer-407 was added to previously prepared NPs suspension. Poloxamer-407 is an

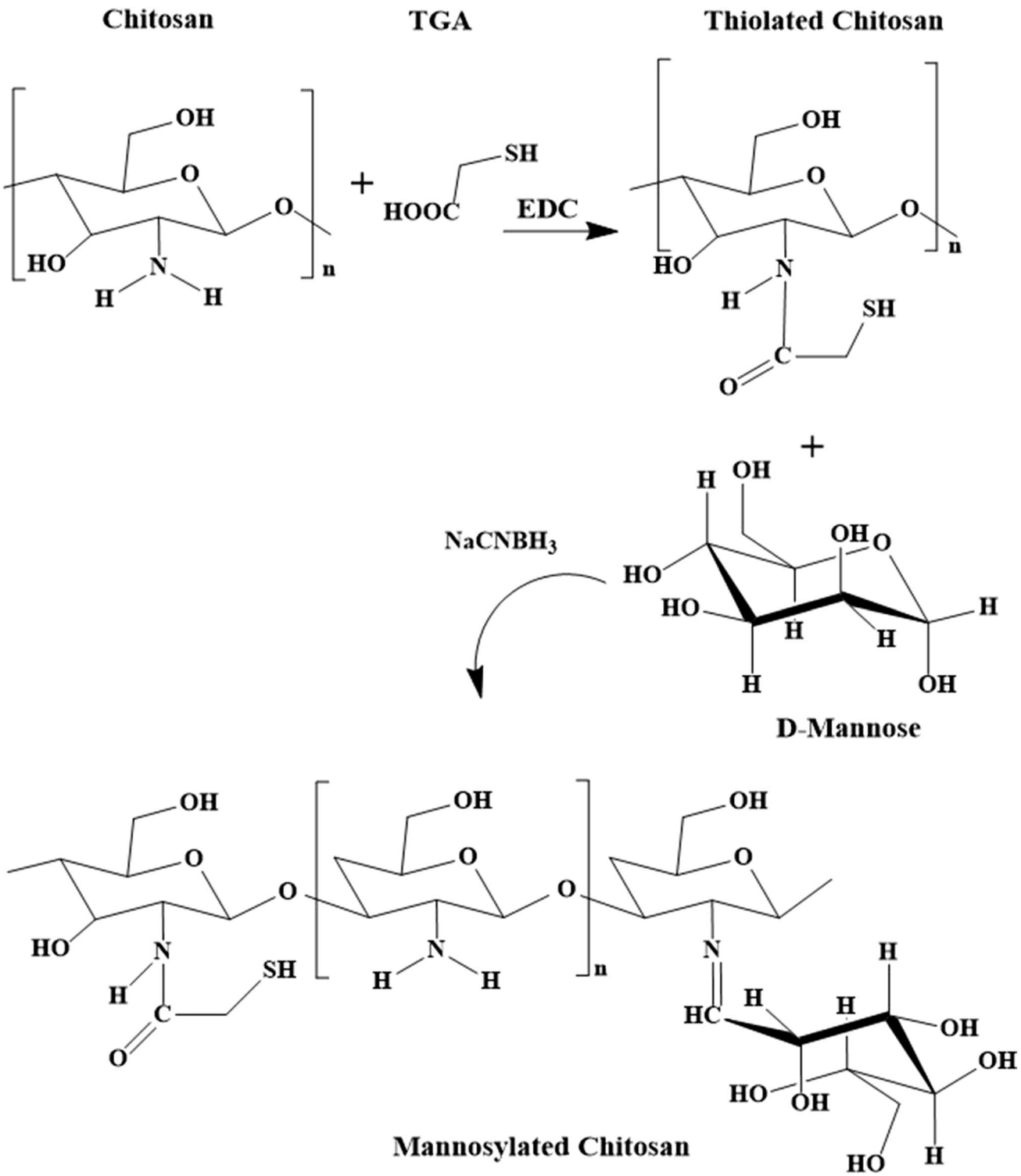

Fig. 1 Schematic pathway for the preparation of mannosylated chitosan (thiolated chitosan synthesis through amide bond formation between the carboxyl group of thioglycolic acid and the amino group of chitosan, then conjugation of mannose group on thiolated chitosan results in the Schiff's base (R–CH=N–R)-mediated amide bond formation between the amino group of thiolated chitosan and aldehyde group of mannose)

amphiphilic surfactant, a tri co-block polymer that acts as an active emulsifier for organic and water phase miscibility and affects the shape and size of NPs (Mazzarino et al. 2012). Afterward, the solution of DEXA and ethanol (1:1) was added dropwise into the above-prepared formulation. This was kept on continuous stirring until the evaporation of the organic phase. After evaporation, MC/DEXA NPs were obtained.

Coating of mannosylated chitosan nanoparticles with ES100

The solvent evaporation technique was used for the coating of prepared nanoparticles (MC/DEXA NPs). Based on the optimization trials, the optimal MC and ES100 concentrations were found to be in a ratio of 1:10. ES100 was dissolved in the co-solvent solution of acetone and IPA (1.5:1) (Chawla et al. 2012), which was then added dropwise to the MC/DEXA NPs solution. The resulting emulsion system was kept on magnetic stirring (1420 rpm) overnight at room temperature until the evaporation of the organic phase (Fig. 3). Afterward, synthesized nano-formulation was centrifuged at 23,000*g* at 4 °C for about half an hour. The obtained pellet was washed twice and re-dispersed in de-ionized water using vortex to remove any residual solvent, though the concentration of class 3 solvent used was very small (ICH 2016). Resulting nanosuspension was later lyophilized and obtained powder was stored at 4 °C for further use. Freeze-drying ensures the physical and chemical stability of prepared nano-formulation and imparts them a good stability.

Optimization of ES100-coated mannosylated chitosan nanoparticles (ES100/MC/DEXA)

Design Expert software (version 7) was used for the optimization of ES100/MC/DEXA NPs. Critical factors affecting the independent variables (average particle size, polydispersity index, and encapsulation efficiency) were screened based on the scientific literature. Dependent variables studied were the concentration of MC, concentration of ES100, and stirring speed. We found response surface central composite design most suitable for the optimization of ES100/MC/DEXA NPs.15 runs was generated by software, evaluating the effect of the dependent variable on independent variables. *p* value, adjusted *R* square, and predicted *R*-square values suggested the quadratic model as the best fit model. Data were evaluated using p and *F* values for confirming model significance. Moreover, surface plots, displaying the interaction between the dependent and independent variables, were obtained from the software (Fig. 2).

Physicochemical characterization

PDI, particle size, and zeta potential

The polydispersity index (PDI) and particle size of nanoparticles were determined by dynamic light scattering using Brookhaven 90Plus (Brookhaven instrument, USA). Zeta potential of nanosuspension was determined by Malvern Zeta sizer 2000 HS (Malvern instrument, UK) before freeze-drying.

Encapsulation efficiency (EE)

Direct drug loading was determined by dispersing the lyophilized powder in 0.5 M GAA, the solvent in which the polymer was solubilized, to disrupt NPs. Solution was stirred to completely evaporate the solvent. Afterward, drug solubilizing solvent (ethanol) was added and stirring was continued for 6 h to completely dissolve the entrapped drug. Then the samples were withdrawn, filtered, and analyzed by UV–visible spectrophotometer at λmax of 240 nm. Percentage of drug loading was obtained by using the Eq. (1).

$$(Direct)\ EE\% = \frac{Actual\ drug\ content\ in\ NPs\ (mg) \times 100}{Theoretical\ drug\ content\ used\ in\ formulation\ (mg)} \quad (1)$$

Indirect drug loading was obtained from supernatant collected after centrifugation at 13,500 rpm for 1 h (Chaubey and Mishra 2014). The sample was analyzed under a UV–visible spectrophotometer at λmax of 240 nm. Percentage EE was then obtained by Eq. (2).

$$(Indirect)\ EE\% = \frac{Total\ drug - free\ drug \times 100}{Total\ drug} \quad (2)$$

Morphological analysis of NPs

SEM images were obtained from a scanning electron microscope (Vega-3, Tescan, USA) to determine the surface and morphology of nanoparticles. Lyophilized dry samples were placed on a silicon wafer and gold-sputtered to make sample conductive. Samples were then viewed at an acceleration voltage of 10 kV.

Differential scanning calorimetry (DSC)

Thermal analysis was carried out with differential scanning calorimetry (Mettler Toledo DSC 821, Mettler Inc., Switzerland) to investigate the physical and chemical changes taking place in NPs. Samples were evaluated for the changes like melting, crystallization, recrystallization, and decomposition. Weighed samples were crimped into aluminum pans which were then heated at a rate of 10 °C/min up to 300 °C.

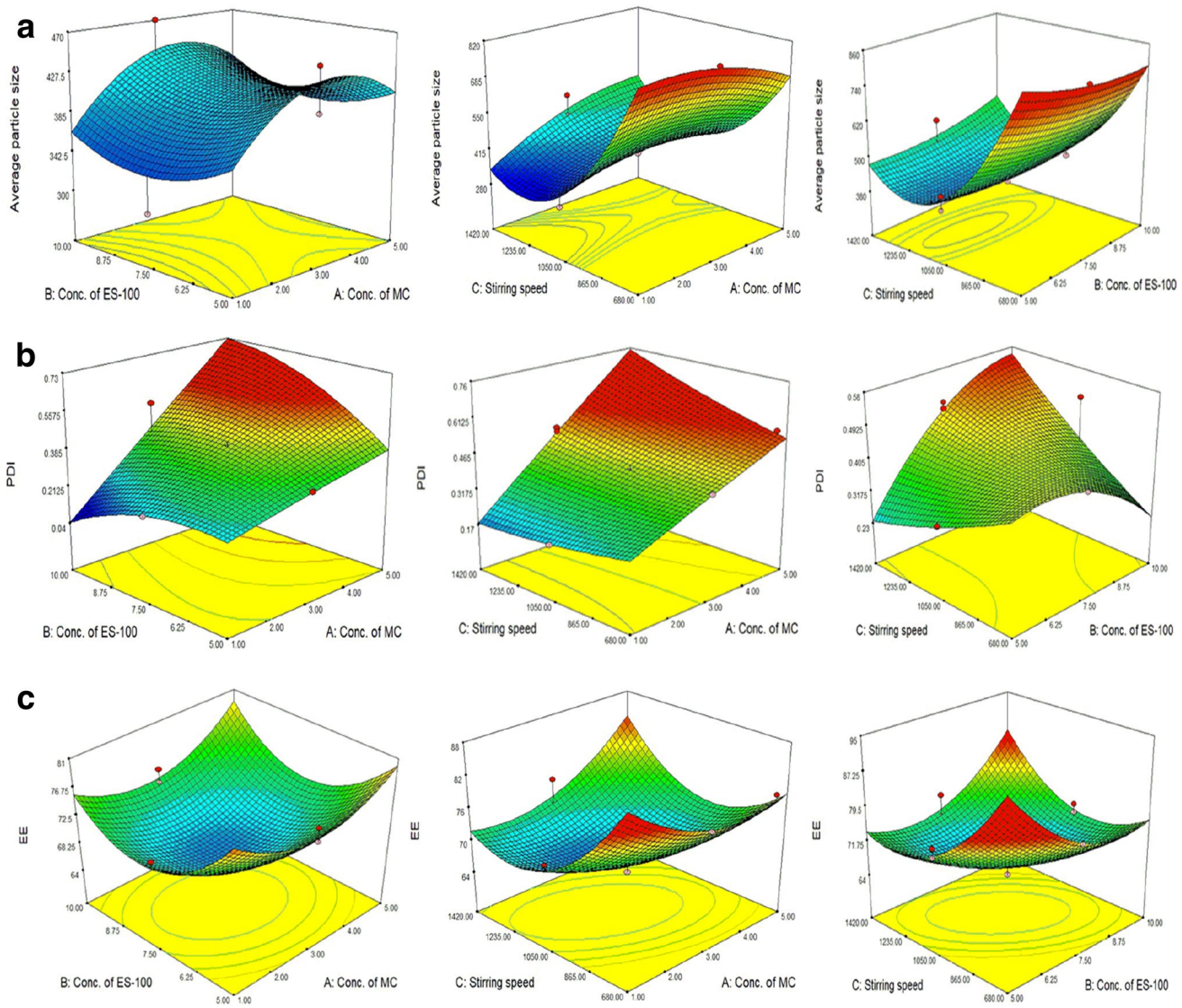

Fig. 2 3D surface plots displaying the impact of different process parameters on average particle size, PDI, and encapsulation efficiency of ES100-coated MC NPs, **a** 3D surface plots showing the combined effect of concentration of MC, concertation of ES100, and stirring speed on particle size; **b** 3D surface plots showing the combined effect of concentration of MC, concertation of ES100, and stirring speed on PDI; **c** 3D surface plots showing the combined effect of concentration of MC, concentration of ES100, and stirring speed on EE

An empty pan was used as a reference with constant gas purging in an inert atmosphere.

Fourier transform infrared spectroscopy (FTIR)

Dry samples of drugs, polymers, and final formulation were analyzed by Fourier transform infrared spectroscopy (Bruker Alpha FTIR spectrophotometer, USA) to determine the physicochemical compatibility between the active drug and polymers in an IR range of 500–4000 cm^{-1}. Furthermore, FTIR was also useful for the confirmation of the thiolation of chitosan and mannose anchoring to the thiolated chitosan.

X-ray photon spectroscopy (XPS)

X-ray photon spectroscopy (XPS) scanning of ES100/MC/DEXA nanoparticles was performed using a Scienta-Omicron system with a micro-focused monochromatic A1 K-Alpha (1486.7 eV) source. X-ray source operated at 15 keV produced the survey scans at 100 eV and 20 eV analyzer energy. The binding energy of the samples was recorded in the range of 0–1200 eV. Samples were prepared on silicon substrates, and charge neutralization was done before the scan to avoid the impact of the charge. Data acquisition and analysis were performed with Matrix software and

Igor pro with XPS fitting procedure. Signal intensities were detected for NPs to confirm the presence of different elements and functional groups on the particles' surface (Baer and Engelhard 2010).

Drug release profile and kinetics modeling

In-vitro drug release

In-vitro release of DEXA from NPs was carried out at pH 1.2 for 2 h and afterward at 7.4 pH for 72 h to simulate GIT conditions. The pH values were chosen because the pH of the colon varies from 1.2–1.5 in the stomach to pH 7–7.8 in the colon. Simulated gastric fluid (SGF) of pH 1.2 and simulated intestinal fluid (SIF) of pH 7.4 were prepared according to United States Pharmacopeia (Ali et al. 2014). 5 mg of freeze-dried MC/DEXA and ES100/MC/DEXA NPs were added to 70 ml of simulated SGF separately. The release profile was assessed for 2 h at pH 1.2 while stirring at a speed of 650 rpm. Afterward, the pH of the medium was adjusted to 7.4 by adding $Na_2HPO_4.2H_2O$, KH_2PO_4, and 0.1 N NaOH to achieve the pH conditions of the colon (Ali et al. 2016). Sink conditions in the release medium were maintained by 0.5% tween 80 (w/v). The release profile was studied for over 72 h. Samples of about 1–2 ml were withdrawn at pre-determined intervals and centrifuged at 24,400*g* for 20 min. The supernatant was then quantified on a UV–visible spectrophotometer at 240 nm wavelength by the method mentioned earlier.

Drug release kinetics

Drug release kinetic models are used for predicting the pattern of drug release from new drug delivery systems. They provide a comparison of physical mechanisms of drug release like diffusion, erosion, etc. and quantifies drug release pattern and behavior. The models can also optimize the dosage of the drug. Different kinetic models including zero-order, first-order, Hixson-Crowell, Higuchi, and Korsmeyer-Peppas were applied to understand drug release patterns and behavior through DD solver software.

The model with the highest value of the coefficient of determination (R^2), adjusted coefficient of determination (adj R^2), and lowest value of Akaike Information Criteria (AIC) was considered the best-fitted model (Zeeshan et al. 2019b).

Biocompatibility assay (MTT)

MTT assay was performed to quantify the mitochondrial activity as a measure of cell viability. Because macrophages were the site of the target, therefore the toxicity of the drug and polymeric NPs was determined on murine-derived macrophages (Tukulula et al. 2015). Murine-derived macrophage cells were cultured on RPMI medium with 10% fetal bovine serum (FBS). In a 48-well plate, viable macrophages were seeded with a density at 5×10^5 cells/well. Afterward, DEXA, MC/DEXA NPs, and ES100/MC/DEXA NPs were incubated at 37 °C with 5% CO_2 supply for 24 h. After 24 h, MTT in a concentration of 500 µg/ml was added, replacing the supernatant and was subjected to incubate for 4 h at 37 °C. 100 µl of DMSO was then added in each plate and cell viability was assessed using a microplate reader at 570 nm wavelength.

Uptake of nanoparticles by murine macrophages

For the uptake study, rhodamine B (Rh-B)-loaded mannosylated chitosan nanoparticles were prepared. Inflammation was induced in mice by intraperitoneal injection of 0.8% acetic acid solution in saline (Niu et al. 2015). Murine macrophages were then harvested by peritoneal lavage. Afterward, the harvested exudate was incubated with DMEM. 200 µl of Rh-B dyed MC nanoparticles were suspended in 1 ml of macrophage exudate. After 2 h of incubation, cellular uptake was observed under a fluorescent microscope to confirm NPs uptake by the macrophages.

Statistical analysis

Statistical analysis was obtained by Microsoft Excel 2013, DD solver, and Sigma plot® 10.0 (Chicago, USA). One way analysis of variance (ANOVA) was applied for the comparison of the drug release profile of uncoated and coated nanoparticles. Each data has been expressed as a mean ± standard deviation (SD). Level of significance was 0.05 ($p < 0.05$).

Results

Synthesis of TC and MC polymers

An amide bond was formed between the carboxyl group of TGA and the amino group of chitosan leading to TC synthesis. Mannose anchoring to thiolated chitosan was facilitated by the Schiff's base-mediated amide bond between aldehyde group of mannose and amino group of TC. Thiol groups immobilized on the CS backbone were then determined and were found to be 462 ± 57 µM per gram of thiolated polymer. The extent of disulfide bond formation due to air oxidation during the polymer modification was assessed. The disulfide bonds were quantified to be 98 ± 26 µM per gram of TC.

The mannose group was then anchored to TC with the reaction between the aldehyde group of mannose and amino group of TC. This successful conjugation reaction was confirmed by the quantification of mannose groups anchored to TC and found to be 254 ± 32 µM per gram of MC. Disulfide

linkage was quantified to be 89 ± 19 µM per gram of MC and number of thiol groups immobilized were calculated to be 386 ± 43 µM per gram of MC, as reported in our previous study (Afzal et al. 2019).

Preparation and optimization of nano-carriers

MC/DEXA nanoparticles were synthesized using the ionic gelation method (Fig. 3). The mean particle size was 300.7 nm ± 11.3 with a PDI of 0.130 ± 0.03. Further, pH-sensitive ES100/MC/DEXA nanoparticles were synthesized with desired attributes, following 15 trials generated by Design Expert. pH-sensitive polymer, ES100 was used as an outer coat to inhibit the premature drug release from nanoparticles in the acidic environment of the GIT. Nanoformulation with MC to ES100 (1:10) and a stirring speed of 1420 rpm was found to be most promising in terms of particle size, PDI, and EE and was used for future investigation. The average particle size was 350.8 nm ± 15.8 with PDI of 0.109 ± 0.01 and EE of 83.1% for ES100/MC/DEXA NPs.

As seen from Fig. 2a, the particle size reduced from 801 to 300 nm by reducing the concentration of MC. However, by increasing the concentration of ES100, a shift toward the reduction of particle size was observed which was more prominent when MC and ES100 were used in a 1:10 ratio. Next, the effect of stirring speed along with the amount of MC on particle size was evaluated. It was found that stirring speed had some effect on the particle size; however, when the concentration of MC was increased along with stirring at high speed, the effect of stirring was not significant. The effect of ES100 together with stirring speed can also be seen in Fig. 2a. As the concentration of ES100 was increased along with reduced stirring speed, there was an increase in average particle size. The optimum speed was found to be 1420 rpm for the decrease in particle size.

It can be observed from Fig. 2b that PDI of ES100-coated NPs was reduced from 0.551 to 0.109 by an increase in the concentration of ES100, which explains the homogenous appearance of the optimized formulation. Furthermore, with an increase in the concentration of MC, a negative shift was observed for PDI, i.e., from small to high values. This holds very true indeed as the formulation with a high amount of MC was found to be aggregated due to higher PDI values. Conversely, PDI value was reduced with an increase in the stirring speed, as the high shear force produced particles with narrow size distribution. However, alternatively, the higher concentration of ES100 had no positive impact on PDI even in the presence of high stirring speed.

The encapsulation efficiency was found to be in the range of 64–83%. By increasing the concentration of MC, there was found to be an increase in the EE from 64 to 83%, as can be seen from Fig. 2c. However, an increase in the concentration of ES100 was not found to be positively correlated to an increase in EE. Stirring speed alone was also found to have no significant effect on the EE. However, the significance

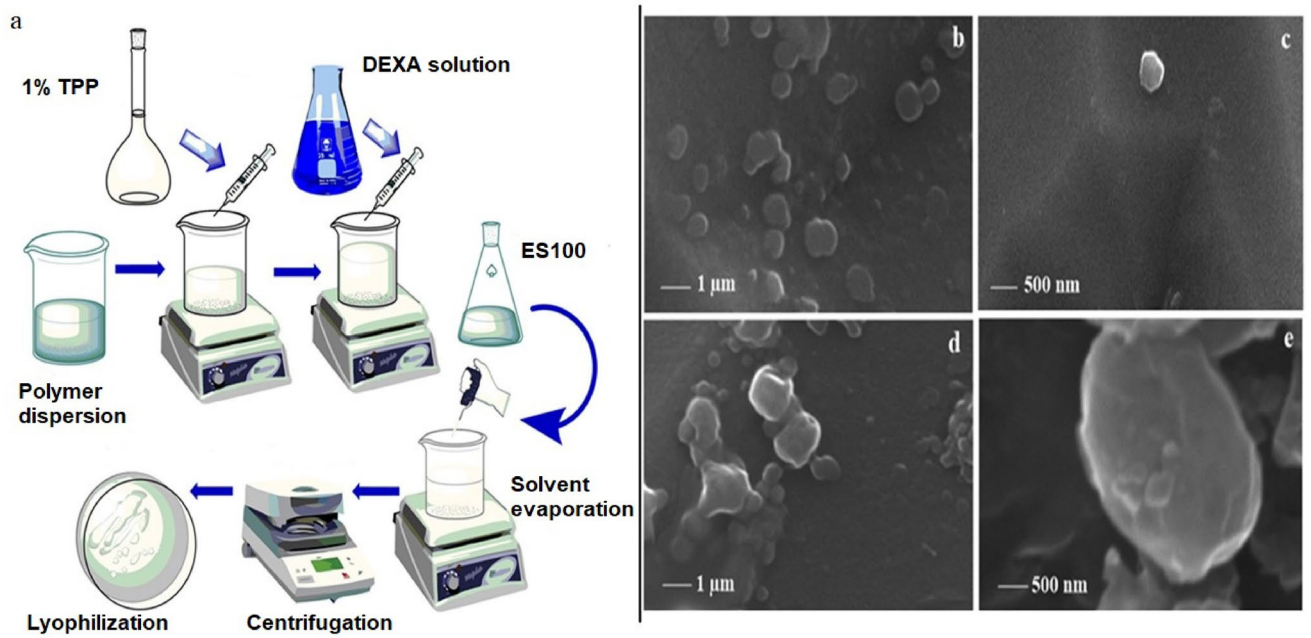

Fig. 3 Preparation of dexamethasone-loaded mannosylated chitosan nanoparticles (MC/DEXA NPs) and pH-sensitive dexamethasone-loaded mannosylated chitosan nanoparticles (ES100/MC/DEXA NPs) (ionic gelation) (**a**), SEM analysis of ES100/MC/DEXA NPs (**b**, **c**) and uncoated MC/DEXA NPs (**d**, **e**)

was more pronounced in the presence of optimal concentrations of MC and ES100.

Zeta potential of ES100/MC/DEXA and MC/DEXA nanosuspensions was − 8.25 ± 6.39 mV and + 20.7 ± 1.2 mV, respectively. The positive charge on the uncoated nanoparticles (MC/DEXA NPs) was mainly due to the presence of cationic polymer, i.e., MC. However, the coating of MC NPs with anionic polymer (ES100), zeta potential of the coated particles became negative. The percentage yield for the ES100/MC/DEXA and MC/DEXA nanoparticles was 63.1 ± 1.3 and 58.8 ± 2.5, respectively. The trials generated, outcome, and significance of various parameters studied with their effect on independent variables are mentioned in online resources.

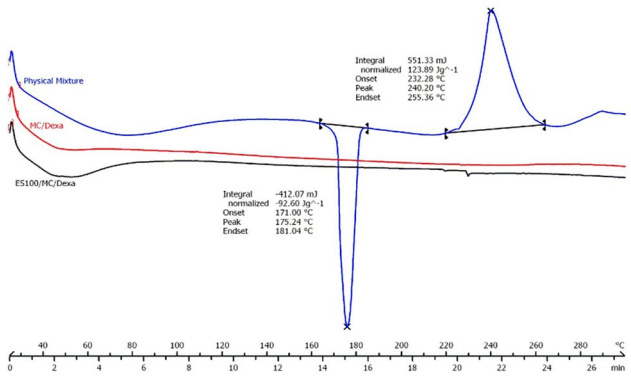

Fig. 4 Differential Scanning Calorimetry (DSC) curve of the physical mixture (DEXA, ES100, MC, TPP), MC/DEXA NPs and ES100 MC/DEXA NPs, Exo↑

Characterization of nano-carriers

Morphological analysis of NPs

The surface morphology was examined through SEM for the dry samples of both the coated and uncoated nanoparticles. MC/DEXA nanoparticles presented the rough surface morphology because the method employed for the synthesis produced a porous matrix-like carriers. Remnants of TPP formed the irregular crystals and particles agglomerated because of electrostatic attraction (Yang et al. 2009). However, ES100/MC/DEXA nanoparticles appeared as smooth spherical carriers, which may suggest the presence of ES100 coat on MC/DEXA NPs (Fig. 3).

Differential scanning calorimetry (DSC)

DSC is one of the methods of assessing information about the physical state of the drug in the final formulation along with the physicochemical interaction between polymers and drugs. DSC curve (Fig. 4) of the physical mixture reveals the melting behavior of drug with a sharp endothermic peak at 175.24 °C. The exothermic peak at 240.20 shows the glass transition temperature (Tg) of ES100. Tg describes the solidification of polymer melt and the absence of Tg peak in the ES100/MC/DEXA NPs suggested that the polymer was compatible with drug and drug was encapsulated in the core of ES100 in an amorphous state (Hu et al. 2012; Katta et al. 2017). Moreover, DSC curves of MC/DEXA NPs and ES100/MC/DEXA NPs did not show any characteristic peaks analogous to physical mixture. The peaks of DEXA disappeared in the DSC curves of NPs indicating that the drug has been wrapped within the core of polymer. This also suggests that the drug has been highly dispersed and entrapped in the amorphous state (previously crystalline) inside the ES100/MC NPs and no recrystallization was observed for both the drug and polymers. Additionally, it could also be inferred that no free drug was present on the surface of the NPs and hence presented no characteristic peak in the NPs.

Fourier transform infrared spectroscopy (FTIR)

FTIR analysis illustrated compatibility between different constituents of the nanoparticles. Additionally, FTIR provides evidence for mannosylation of thiolated chitosan. Therefore, the FTIR spectrum of mannosylated chitosan (Fig. 5a) shows a characteristic peak at 3351.69 cm^{-1} corresponding to the amide bond stretch and another fingerprint peak at 1032.73 cm^{-1} shows the NH_2 band (Shahnaz et al. 2017). OH functional group stretch at 3500 cm^{-1}, CH_2 bond widening at 2900 cm^{-1}, C=O bond formation at 1723 cm^{-1}, and an axial CF bond at 510 cm^{-1} confirm the presence of DEXA core in the prepared ES100/MC/DEXA NPs. MC displays an amide bond formation peak at 1100 cm^{-1} and OH bond stretch and NH_2 group at 1530 cm^{-1}, in the spectrum of the NPs. Coating polymer, ES100, was confirmed as an intact coat shell, which can be noted by the carboxyl bond stretch at 1149 cm^{-1} and 1723 cm^{-1}. CH_3 bend at 1437 cm^{-1}, C-CH_2 bond stretch at 2928 cm^{-1}, and –C=O–bond widening at 1723 cm^{-1} equally confirmed the presence of ES100 (Thakral et al. 2010).

X-ray photon spectroscopy (XPS)

The XPS spectra as shown in Fig. 5 have been collected from synthesized ES100/MC/DEXA nanoparticles. In the survey scan of XPS analysis, only the peaks of carbon and oxygen were observed. The surface composition of carbon and oxygen was 60.67% and 33.33%, respectively, for the ES100/MC/DEXA nanoparticles (Table 1-A). Since XPS is a highly sensitive and precise technique (~ 10 nm) and it did not trace the presence of nitrogen and sulphur in the samples. Nitrogen and sulphur are the constituents of MC (Fig. 1); therefore,

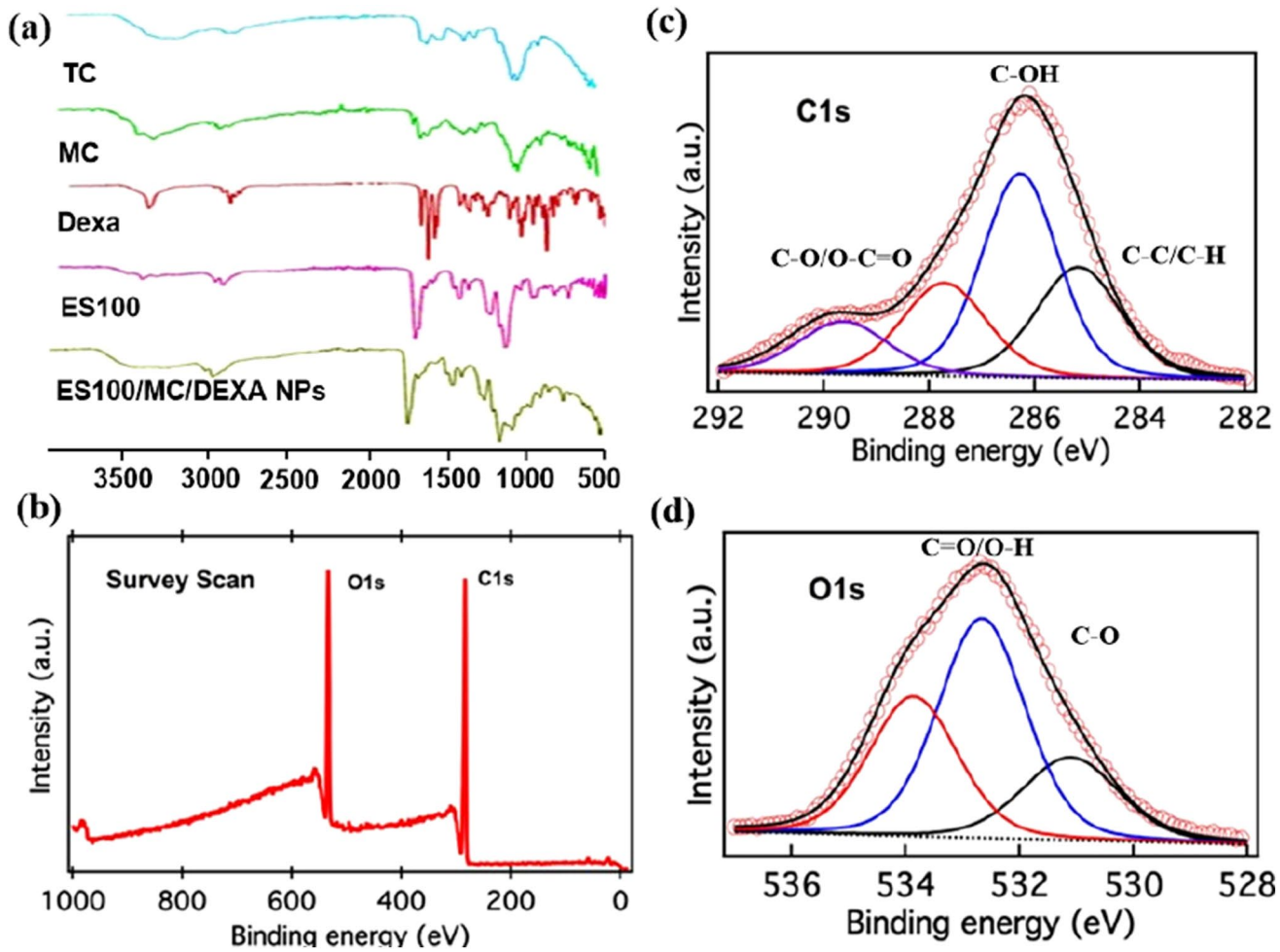

Fig. 5 **a** Fourier transform infrared spectroscopy (FTIR) spectra of thiolated chitosan, mannosylated chitosan, dexamethasone, ES100, ES100-coated mannosylated chitosan NPs. Amide, carbonyl and hydroxyl groups confirm the immobilization of thiol and mannose. **b** X-ray photon spectroscopy (XPS) survey scan for detection of elements present on the surface, **c** C1s core-level spectra for analysis of functional groups with carbon, **d** O1s core-level spectra for detection of oxygen-containing functional groups

Table 1 (A) % of elements present on the surface of ES100-coated MC nanoparticles. (B) Functional groups detected by XPS analysis at O1s and C1s spectra of ES100-coated MC nanoparticles

(A) Atomic percentage of elements on surface				
C	O	N	S	
60.67	37.33	0	0	
(B) O1s and C1s spectra				
O1s core level	C–O	C=O	O–H	
Binding energy (eV)	531.2	532.7	533.72	
Atomic percentage (at. %)	19.10	53.80	27.10	
C1s core level	C–C/C–H	C–OH	C–O	O-C=O
Binding energy (eV)	285	286.3	287.8	289.7
	25.11	41.29	21.05	12.53

the absence of 'N' and 'S' ensures a layer of ES100 on the surface of MC/DEXA NPs. ES100 does not contain such elements in its structure, thereby confirming that the nanoparticles have been coated successfully with ES100.

O1s and C1s photoemission core levels were obtained for detailed analysis of functional groups present on the surface of the nanoparticles. The O1s spectrum of ES100/MC/DEXA nanoparticles is resolved into three sub-peaks located at 531.2 eV, 532.7 eV, and 533.7 eV, which characteristically belong to C–O, C=O, and OH, respectively. C1s spectra for ES100/MC/DEXA NPs is resolved into four sub-peaks: 285 eV, 286.3 eV, 287.8 eV, and 289.7 eV (Fig. 5, Table 1-B). These sub-peaks belong to C–C/C–H, C–OH, C=O, and O–C=O functional groups, respectively. Therefore, XPS spectra revealed the presence of ES100 on the surface of nanoparticles by the detection of alkyl, carboxylic OH, esteric CO, and acidic/esteric C=O groups, which are main composition elements of coating polymer (ES100) (Davies et al. 1989).

Drug release and kinetics of drug release

In-vitro drug release

In-vitro drug release from MC/DEXA and ES100/MC/DEXA NPs was studied in a pH changing medium. At first, the MC/DEXA and ES100/MC/DEXA NPs were incubated at pH 1.2 for 2 h. Afterward, the pH of the medium was adjusted to 7.4, and the experiment was continued for 72 h (Fig. 6). The uncoated NPs showed burst release in the first 2 h at pH 1.2 which was later a sustained release with no effect of pH change. 28.8% DEXA was released in the first 2 h indicating that uncoated NPs are prone to drug release at acidic pH and can release maximum drug within few hours in the colon. The premature and burst release of drug in the stomach may lead to the unwanted adverse effects and insufficient drug delivery to the colon. In contrast, ES100 /MC/DEXA NPs exhibited a pH-dependent release profile with minimal drug release (about 1%) at pH 1.2 followed by sustained release at pH 7.4. The coating with ES100 inhibited the burst release of the drug at the acidic pH and over 73.9% of drug was released over 72 h. These results highlight that ES100-coated NPs have the potential to retain the drug until reaching the colon, which is a promising approach for colon-targeted drug delivery.

ANOVA described the statistical significance between the drug release profiles of ES100/MC/DEXA and MC/DEXA NPs with $p < 0.05$ and F-value > F-critical value. A comparison of profiles demonstrated the difference between the release pattern of the drug from uncoated and coated NPs.

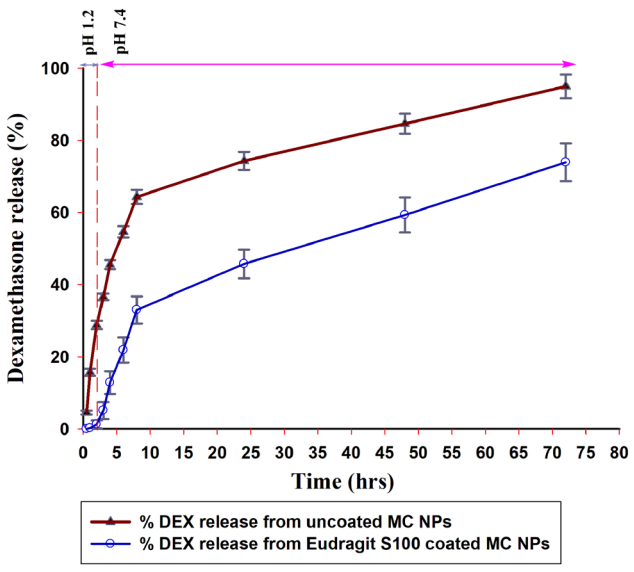

Fig. 6 In-vitro release of dexamethasone from uncoated and coated nanoparticles in simulated gastrointestinal fluid, at pH 1.2 and pH 7.4 ($n = 3 \pm$ SD)

Drug release kinetics

Mathematical models were applied to understand the mechanism and kinetics of drug release (Table 2). Each model signifies the pattern of drug release, though with certain limitations. As the nano-carrier is a complex entity, therefore, more than one model explains drug release virtually. Different models were selected based on R^2, adj R^2, and AIC. MC/DEXA NPs were found best fitted to Korsemeyer-Peppas, whereas ES100/MC/DEXA NPs were best fitted to Korsemeyer-Peppas > Higuchi. Both MC/DEXA NPs and ES100/MC/DEXA NPs followed Korsmeyer-Peppas model. Value of n (0.315) for MC/DEXA NPs is describing the Fickian drug diffusion, whereas the value of n (0.579) for ES100/MC/DEXA NPs describes the anomalous non-Fickian diffusion which refers to the combination of diffusion and erosion-controlled drug release from polymeric core (Sriamornsak et al. 2007). As the nano-carrier system becomes complex after coating with pH-sensitive polymer, so the shift occurs from Fickian to non-Fickian diffusion. For ES100/MC/DEXA NPs, the Higuchi model justifies the gradual release of drugs based on the function of the unit surface area of NPs (Bruschi 2015). As the nano-carrier system undergoes erosion, the cumulative surface area increases which facilitates the efficient and sustained release of drugs. Moreover, this model is descriptive of the maintenance of sink conditions during the release study. All these findings are found accurate to the research rationale, which is the release of drug in colon at sustained rate as a combined function of swelling, solubility of carboxylic group of polymeric side chain in alkaline pH and diffusion across the pH sensitive coat.

Table 2 Kinetic models for release profile of MC/DEXA NPs and ES100/MC/DEXA NPs

Model	Parameters	MC/DEXA NPs	ES100/MC/DEXA NPs
Zero order	R^2	0.663	0.871
	adj R^2	0.625	0.857
	AIC	93.592	78.779
	MSC	0.494	1.436
	K_0	1.099	1.042
1st order	R^2	0.919	0.93
	adj R^2	0.919	0.93
	AIC	75.725	70.218
	MSC	2.136	2.225
	K_1	0.133	0.023
Higuchi	R^2	0.779	**0.937**
	adj R^2	0.779	**0.937**
	AIC	87.227	68.877
	MSC	1.073	2.336
	K_h	13.562	8.577
Korsmeyer-Peppas	R^2	**0.927**	**0.948**
	adj R^2	**0.919**	**0.942**
	AIC	76.752	68.837
	MSC	2.025	2.339
	K_{kp}	26.063	6.512
	N	**0.315**	**0.579**
Hixson-Crowell	R^2	0.712	0.901
	adj R^2	0.712	0.901
	AIC	89.844	73.830
	MSC	0.859	1.886
	K_{hc}	0.021	0.006

The best fitted models are mentioned in bold for the uncoated and coated nanoparticles

*R2 = coefficient of determination, adj R2 = adjusted coefficient of determination, Akaike information criterion, MSC = model selection criterion, k = rate constant, n = release exponent

Biocompatibility assay (MTT)

The biocompatibility of the drug and nanoparticles was evaluated with isolated murine macrophages at three different concentrations of DEXA and nanoformulations as the equivalent concentration of 50, 75, 100 µg/ml of dexamethasone, after 24 h of incubation. The concentration of 100 µg/ml was chosen for nano-formulation used for study. Results are expressed as mean ± SD in Fig. 7. The percentage cell viability of formulations at a concentration of 100 µg/ml was compared. The ranking order of biocompatibility was ES100/MC/DEXA NPs > MC/DEXA NPs > DEXA. Percentage cell viability was found to be highest for ES100/MC/DEXA NPs, i.e., 94.8% ± 3.68. Positive control (media with fetal calf serum) and negative control (Triton X 100) showed 100% ± 0.57 and 2.84% ± 1.46 and were used to maintain the accuracy of the assay.

Uptake study of nanoparticles in murine macrophages

Fluorescence microscopic image revealed that mannosylated chitosan nanoparticles dyed with Rh-B were efficiently taken up by the murine macrophages. Cells were imaged with a Leica fluorescence microscope at 40 × objective magnification. Accumulation of Rh-B-loaded nanoparticles inside macrophages is evident in Fig. 7. It has been established that particles larger than 100 nm in size are most favorably phagocytosed by the macrophages (Weissleder et al. 2014). Positive zeta potential of the nanoparticles (MC/DEXA NPs) after the disintegration of coating on reaching the colon favors the engulfment of the nanoparticles inside themacrophages (Hoshyar et al. 2016). Both the size and charge were optimum for the prepared nanoformulation.

Discussion

However, the main issue with conventional dosage forms, designed for IBD, is the inability to deliver the required dose of the drug to the inflamed area of the colon because of elevated mucin production, increased drug clearance, inefficient targeting to the inflamed area and first-pass effect. Therefore, modulation of cellular events with promising therapeutic approaches is possible by employing nanotechnology. Nanoparticles have prolonged residence time in GIT, making them a promising carrier for drug delivery in the treatment of IBD (Pertuit et al. 2007). The role of macrophages in IBD has been established by extensive investigation in the recent times. As macrophages are involved in the progression of the diseased state, macrophages may serve as a potential therapeutic target because of the overexpression of different key receptors on their surface. The potential of pH-sensitive polymer (Eudragit L100)-coated mannosylated chitosan-based NPs have been investigated in the past, as an oral vaccine-targeting antigen-presenting cells in Peyer's patches in the small intestine (Xu et al. 2018). However, here we hypothesize the possible efficiency of targeted vehicles capable of delivering anti-inflammatory drugs locally to the macrophages in the distal colon using ES100. MR on macrophages has a high affinity for the sulfated and mannosylated moieties. Thus, the functional properties of chitosan were enhanced by anchoring mannose to the polymer backbone, to synthesize MC which is biocompatible as well as biodegradable. Furthermore, ES100-coated MC nano-carrier system was formulated to prevent pre-mature drug release and prolong the sustained release of DEXA in

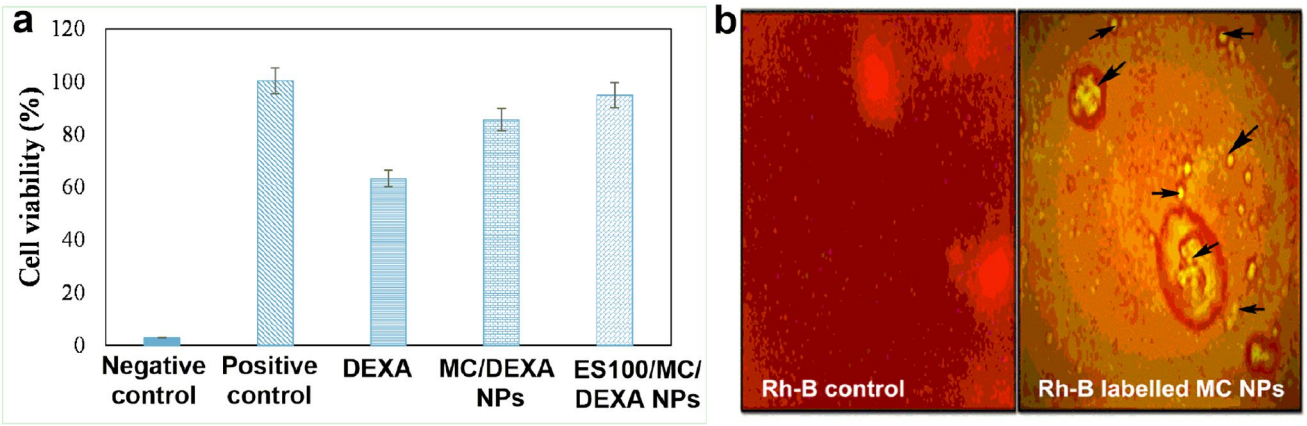

Fig. 7 **a** Biocompatibility of dexamethasone and nanoparticles evaluated in murine macrophages after 24 h of incubation. The concentration of 100 µg/ml of dexamethasone was chosen for nanoparticles studied. Statistical significance of $p < 0.005$ was observed for the results expressed as mean ($n = 3 \pm$ SD); **b** Uptake of rhodamine-B labeled nanoparticles; fluorescence microscopic images were obtained at 40X magnification. Control being untreated macrophages (left), Rh-B-loaded MC nanoparticles (right), which were incubated with freshly harvested murine macrophages for 2 h

the inflamed tissues of colon for active targeting of infiltrated macrophages in the colon.

MC/DEXA NPs were synthesized by a cost-effective ionic gelation method, which involved interaction between positively charged MC and negatively charged TPP molecules (Shahnaz et al. 2017). DEXA was encapsulated in the nano-carriers to overcome the dose-dependent toxicity of DEXA. And the encapsulation efficiency was found to be relatively high because of its hydrophobic nature. Further, pH-sensitive NPs were optimized by Design Expert software to evaluate the critical factors affecting the final product. The method of coating of mannosylated chitosan NPs with ES100 was reported for the very first time in this work, developed with a co-solvent mixture of acetone and IPA (1.5:1) using solvent evaporation technique. 1 N NaOH solution and ethyl acetate solution were also tested individually as a dispersion media for ES100 in the method mentioned above. However, a precipitated suspension was formed with 1 N NaOH, probably because of the drop in zeta potential. Moreover, phase separation was observed with ethyl acetate as a coating solvent, due to the separation of ethylacetate from ethanol. This phase separation was due to the presence of ethanol, as a drug solvent, in the presence of hydrophilic solvent (glacial acetic acid-based MC solubilizing medium) (Zhang et al. 2008). Initially, the ES-100 coat was investigated using drug release studies, for which MC/DEXA NPs and ES100/MC/DEXA NPs were dispersed in the SGF (pH 1.2) followed by a change of media to SIF (pH 7.4). A noticeable percentage of the drug was released at pH 1.2 from uncoated NPs; however, negligible drug release was observed upon subsequent coating of ES100 on MC/DEXA NPs (Fig. 6). A sudden burst release was detected in SIF (pH 7.4) because of the deprotonation of the carboxylic group of ES100 in the alkaline phase. Hence, ES100 has carboxyl and ester groups, making it more soluble at pH 7.4 rather than lower pH. Further, the coating was mechanistically justified by the non-Fickian drug release from ES100/MC/DEXA NPs as the coating polymer dissolved over time in the SIF (Fu and Kao 2010). Drug release patterns from ES100/MC/DEXA and MC/DEXA NPs were compared statistically and found to be significantly different ($p < 0.05$; $F > F$-critical). Additionally, XPS provided scientific evidence of pH-sensitive coating on MC/DEXA NPs. Indeed, the binding energies at the atomic level and surface elemental composition (Fig. 5; Table 1), confirmed our hypothesis of successful coating with ES100. XPS technique is highly sensitive; it can detect the small physical changes in the composition by electrons' movement over a very small distance in the material without losing free energy.

NPs were later analyzed for particle size and surface charge. SEM micrographs revealed that NPs were spherical in morphology. Zeta sizer confirmed narrow particle size distribution with the surface charge of $+20.7 \pm 1.2$ mV on MC/DEXA NPs, since MC polymer has a zeta potential of $+14$ to $+22$ mV. The cationic surface charge of MC/DEXA NPs on subsequent coating with ES100 shifted toward anionic surface charge, -8.25 ± 6.39 mV(Chaubey et al. 2014). Additionally, FTIR analysis highlighted compatibility between the different constituents of the formulation (Fig. 5). DEXA core was intact inside MC and ES100, as characterized by FTIR spectra. Moreover, FTIR spectra confirmed the successful derivatization of chitosan to MC.

The biocompatibility of the formulations was assessed and found to be in the order of ES100/MC/DEXA NPs > MC/DEXA NPs > DEXA. This highlighted that the entrapment of drug inside the polymeric matrix reduces

its toxicity and exposure to viable cells. Mannosylation of polymer improved biocompatibility profile because it reduced the number of available charged amino groups (Afzal et al. 2019), as they are responsible for interaction with the membrane proteins, thereby producing toxicity. A significant decline in the toxicity with ES100 coating can be observed ($p < 0.005$). Besides, uptake of Rh-B NPs by murine macrophages showed that the nano-carriers have a therapeutic potential in actively targeting the immunological cells, involved in the pathogenesis of IBD. This research study summed up the optimum drug release profile for the colon-targeted drug delivery along with the various justified *in-vitro* characterization techniques to be a better therapy for IBD. The study serves as a platform to further elucidate high drug content release in the colon from the NPs without any premature release in the stomach and uptake into infiltrated macrophages at colon in the animal models of IBD. The evidence from this study suggests that a developed nano-carrier system may have an affinity for polarized macrophages at the inflamed colon. The mannosylated chitosan can be further explored as a potential therapeutic drug delivery vehicle for diseases of the colon.

Conclusion

In this work, the pH-responsive mannosylated nano-carrier system was prepared by ionic gelation by software-driven optimization following the quadratic model. The prepared NPs exhibited a pH-dependent release profile for 72 h in colon avoiding premature release of dexamethasone in the upper GI tract. The in-vitro characterization provided data for the delivery of NPs in IBD by oral route. Furthermore, cell viability study reported biocompatibility of the prepared NPs. It can be postulated from the obtained data that this might be a novel approach in actively targeting macrophages at the molecular level. Moreover, the present study has a great reference value for targeted drug delivery in IBD. However, detailed in-vivo studies on relevant animal models would be essential to further explore the therapeutic effectiveness of this novel drug delivery system.

Funding This research did not receive any specific grant from funding agencies in the public, commercial, or not-for-profit sectors.

Compliance with ethical standards

Conflict of interest The authors declare that they have no conflict of interest.

References

Afzal I, Sarwar HS, Sohail MF, Varikuti S, Jahan S, Akhtar S, Yasinzai M, Satoskar AR, Shahnaz G (2019) Mannosylated thiolated paromomycin-loaded PLGA nanoparticles for the oral therapy of visceral leishmaniasis. Nanomedicine 14:387–406

Akira S, Uematsu S, Takeuchi O (2006) Pathogen recognition and innate immunity. Cell 124:783–801

Ali H, Weigmann B, Neurath M, Collnot E, Windbergs M, Lehr C-M (2014) Budesonide loaded nanoparticles with pH-sensitive coating for improved mucosal targeting in mouse models of inflammatory bowel diseases. J Control Release 183:167–177

Ali H, Weigmann B, Collnot E-M, Khan SA, Windbergs M, Lehr C-M (2016) Budesonide loaded PLGA nanoparticles for targeting the inflamed intestinal mucosa—pharmaceutical characterization and fluorescence imaging. Pharm Res 33:1085–1092

Baer DR, Engelhard MH (2010) XPS analysis of nanostructured materials and biological surfaces. J Electron Spectrosc Relat Phenom 178:415–432

Beaugerie L, Langholz E, Nyboe-Andersen N, Pigneur B, Sokol H, Epicom E (2018) Differences in epidemiological features between ulcerative colitis and Crohn's disease: the early life-programmed versus late dysbiosis hypothesis. Med Hypotheses 115:19–21

Bernkop-Schnürch A, Schwarz V, Steininger S (1999) Polymers with thiol groups: a new generation of mucoadhesive polymers? Pharm Res 16:876–881

Bruschi ML (2015) Mathematical models of drug release. Strategies to modify the drug release from pharmaceutical systems. Woodhead Publishing, Cambridge, p 63

Chakraborty P, Ghosh D, Basu MK (2001) Modulation of macrophage mannose receptor affects the uptake of virulent and avirulent Leishmania donovani promastigotes. J Parasitol 87:1023–1027

Chaubey P, Mishra B (2014) Mannose-conjugated chitosan nanoparticles loaded with rifampicin for the treatment of visceral leishmaniasis. Carbohyd Polym 101:1101–1108

Chaubey P, Patel RR, Mishra B (2014) Development and optimization of curcumin-loaded mannosylated chitosan nanoparticles using response surface methodology in the treatment of visceral leishmaniasis. Expert Opin Drug Deliv 11:1163–1181

Chawla A, Sharma P, Pawar P (2012) Eudragit S-100 coated sodium alginate microspheres of naproxen sodium: formulation, optimization and in vitro evaluation. Acta Pharm 62:529–545

Davies M, Wilding I, Short R, Khan M, Watts J, Melia C (1989) An analysis of the surface chemical structure of polymethacrylate (Eudragit) film coating polymers by XPS. Int J Pharm 57:183–187

Dehshahri A, Oskuee RK, Ramezani M (2012) Plasmid DNA delivery into hepatocytes using a multifunctional nanocarrier based on sugar-conjugated polyethylenimine. Gene Ther Mol Biol 14:62–71

Fu Y, Kao WJ (2010) Drug release kinetics and transport mechanisms of non-degradable and degradable polymeric delivery systems. Expert Opin Drug Deliv 7:429–444

Giron F, Pastó A, Tasciotti E, Abraham BP (2019) Nanotechnology in the treatment of inflammatory bowel disease. Inflamm Bowel Dis 25(12):1871–1880

Hatami E, Mu Y, Shields DN, Chauhan SC, Kumar S, Cory TJ, Yallapu MM (2019) Mannose-decorated hybrid nanoparticles for enhanced macrophage targeting. Biochem Biophys Rep 17:197–207

Hoshyar N, Gray S, Han H, Bao G (2016) The effect of nanoparticle size on in vivo pharmacokinetics and cellular interaction. Nanomedicine 11:673–692

Hu D, Liu L, Chen W, Li S, Zhao Y (2012) A novel preparation method for 5-aminosalicylic acid loaded Eudragit S100 nanoparticles. Int J Mol Sci 13:6454–6468

ICH, I. G. Q3c (R6) (2016) on Impurities: guideline for residual solvents. International conference for harmonisation of technical requirements for registration of pharmaceuticals for human use (ICH), Switzerland, 2016

Katta R, Deveswaran R, Bharath S, Basavaraj B (2017) Development of mesalazine microspheres for colon targeting. J Pharm Res 9:1–9

Mazzarino L, Travelet C, Ortega-Murillo S, Otsuka I, Pignot-Paintrand I, Lemos-Senna E, Borsali R (2012) Elaboration of chitosan-coated nanoparticles loaded with curcumin for mucoadhesive applications. J Colloid Interface Sci 370:58–66

Mukhtar M, Ali H, Ahmed N, Munir R, Talib S, Khan AS, Ambrus R (2020) Drug delivery to macrophages: A review of nano-therapeutics targeted approach for inflammatory disorders and cancer. Expert Opin Drug Deliv. https://doi.org/10.1080/17425247.2020.1783237

Niu X, Zhang H, Li W, Mu Q, Yao H, Wang Y (2015) Anti-inflammatory effects of cavidine in vitro and in vivo, a selective COX-2 inhibitor in LPS-induced peritoneal macrophages of mouse. Inflammation 38:923–933

Pertuit D, Moulari B, Betz T, Nadaradjane A, Neumann D, Ismaïli L, Refouvelet B, Pellequer Y, Lamprecht A (2007) 5-Amino salicylic acid bound nanoparticles for the therapy of inflammatory bowel disease. J Control Release 123:211–218

Sartor RB (2006) Mechanisms of disease: pathogenesis of Crohn's disease and ulcerative colitis. Nat Rev Gastroenterol Hepatol 3:390

Shahnaz G, Edagwa BJ, McMillan J, Akhtar S, Raza A, Qureshi NA, Yasinzai M, Gendelman HE (2017) Development of mannose-anchored thiolated amphotericin B nanocarriers for treatment of visceral leishmaniasis. Nanomedicine (Lond) 12:99–115

Sriamornsak P, Thirawong N, Weerapol Y, Nunthanid J, Sungthongjeen S (2007) Swelling and erosion of pectin matrix tablets and their impact on drug release behavior. Eur J Pharm Biopharm 67:211–219

Tams Todd RT (2003) Diseases of the stomach. In: Handbook of small animal gastroenterology. W B Saunders Company, pp 159–194

Thakral NK, Ray AR, Majumdar DK (2010) Eudragit S-100 entrapped chitosan microspheres of valdecoxib for colon cancer. J Mater Sci Mater Med 21:2691–2699

Tukulula M, Hayeshi R, Fonteh P, Meyer D, Ndamase A, Madziva MT, Khumalo V, Lubuschagne P, Naicker B, Swai H (2015) Curdlan-conjugated PLGA nanoparticles possess macrophage stimulant activity and drug delivery capabilities. Pharm Res 32:2713–2726

Vafaei SY, Esmaeili M, Amini M, Atyabi F, Ostad SN, Dinarvand R (2016) Self assembled hyaluronic acid nanoparticles as a potential carrier for targeting the inflamed intestinal mucosa. Carbohyd Polym 144:371–381

Weissleder R, Nahrendorf M, Pittet MJ (2014) Imaging macrophages with nanoparticles. Nat Mater 13:125

Xu B, Zhang W, Chen Y, Xu Y, Wang B, Zong L (2018) Eudragit® L100-coated mannosylated chitosan nanoparticles for oral protein vaccine delivery. Int J Biol Macromol 113:534–542

Yang W, Fu J, Wang T, He N (2009) Chitosan/sodium tripolyphosphate nanoparticles: Preparation, characterization and application as drug carrier. J Biomed Nanotechnol 5:591–595

Zeeshan M, Ali H, Khan S, Khan SA, Weigmann B (2019a) Advances in orally-delivered pH-sensitive nanocarrier systems; an optimistic approach for the treatment of inflammatory bowel disease. Int J Pharm 558:201–214

Zeeshan M, Ali H, Khan S, Mukhtar M, Khan MI, Arshad M (2019b) Glycyrrhizic acid-loaded pH-sensitive poly-(lactic-co-glycolic acid) nanoparticles for the amelioration of inflammatory bowel disease. Nanomedicine 14:1945–1969

Zhang DL, Deng YF, Li CB, Chen J (2008) Separation of ethyl acetate− ethanol azeotropic mixture using hydrophilic ionic liquids. Ind Eng Chem Res 47:1995–2001